www.sciencemag.org/content/351/6270/275/suppl/DC1

Supplementary Materials for

AMP-activated protein kinase mediates mitochondrial fission in response to energy stress

Erin Quan Toyama,* Sébastien Herzig,* Julien Courchet, Tommy L. Lewis Jr., Oliver C. Losón, Kristina Hellberg, Nathan P. Young, Hsiuchen Chen, Franck Polleux, David C. Chan, Reuben J. Shaw†

*These authors contributed equally to this work.
†Corresponding author. E-mail: shaw@salk.edu

Published 15 January 2016, *Science* **351**, 275 (2016)
DOI: 10.1126/science.aab4138

This PDF file includes:

Materials and Methods
Supplementary Text
Figs. S1 to S7
Full Reference List
Captions for Movies S1 to S5

Other Supplementary Material for this manuscript includes the following:
(available at www.sciencemag.org/content/351/6270/275/suppl/DC1)

Movies S1 to S5

Toyama, Herzig et al. Supplemental Materials:

Supplemental Figures S1 to S7

Movies S1 to S5

Movie S1: WT U2OS stained with Mitotracker Green and treated with 250ng/ml Rotenone.

Movie S2: AMPK DKO U2OS stained with Mitotracker Green and treated with 250ng/ml Rotenone

Movie S3: WT U2OS stained with Mitotracker Green and treated with vehicle (DMSO)

Movie S4: WT U2OS stained with Mitotracker Green and treated with 300⌈M A769662

Movie S5: AMPK DKO U2OS stained with Mitotracker Green and treated with 300⌈M A769662

Materials and Methods

Supplemental Text re: MFF alternative splicing

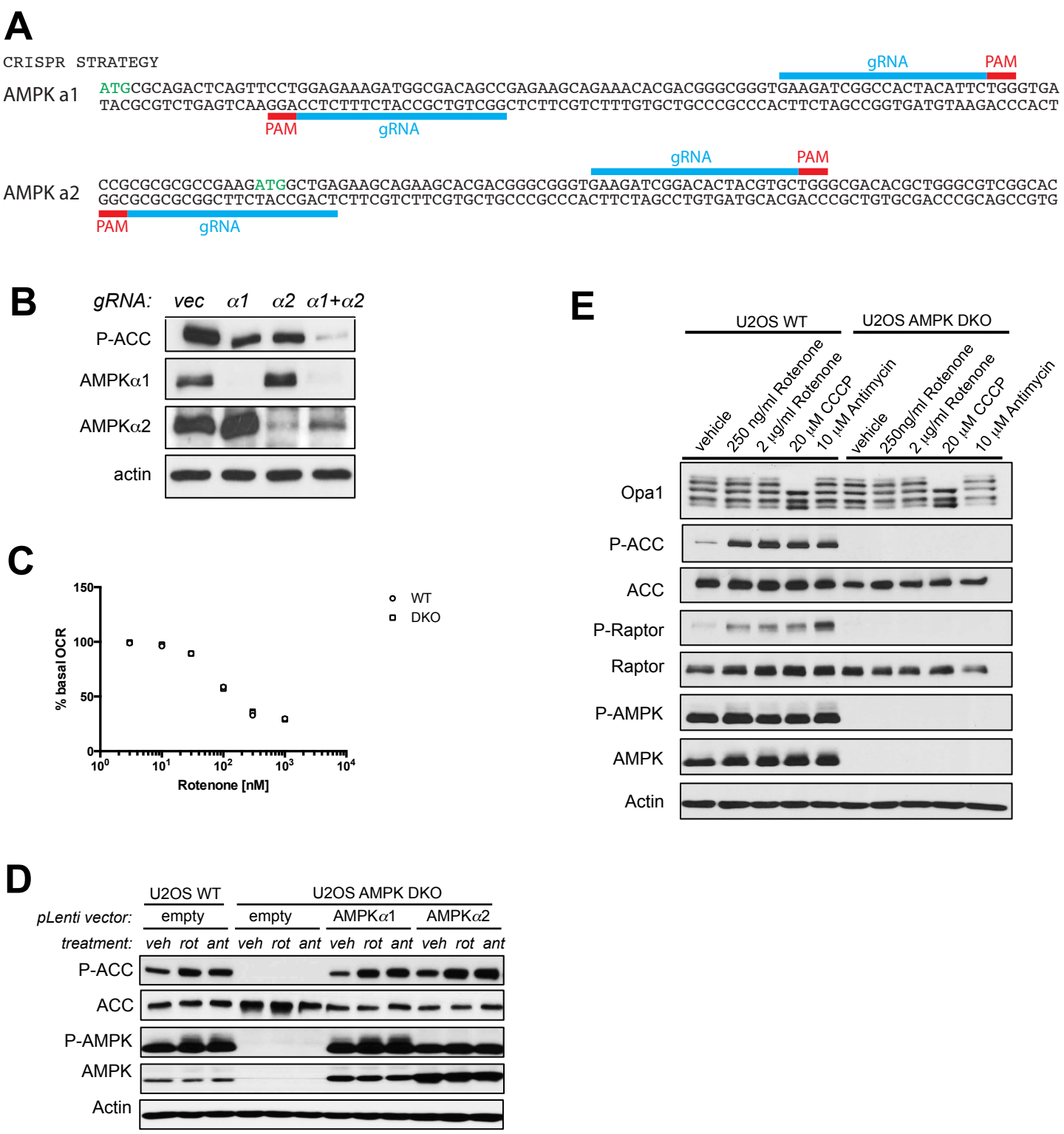

Fig. S1. Creation of AMPKα1,α2 CRISPR/Cas9 DKO cell lines and study of response to ETC inhibitors.
(**A**) Schematic representation of the DNA sequence targeted by the guide RNA pairs against AMPK α1 and α2.
(**B**) Protein immunoblot of U2OS cells transfected with the indicated guide RNA pairs and selected with puromycin.
(**C**) Dose response of Oxygen Consumption Rate (OCR) in WT or AMPK DKO U2OS cells with increasing concentration of Rotenone.
(D) Protein immunoblot of the cell lines and conditions shown in Figure 1A. veh: Vehicle (DMSO), rot: 250ng/ml Rotenone, ant: 10μM Antimycin A.
(**E**) Analysis of OPA1 processing by protein immunoblot in WT and AMPK DKO U2OS cells after 1 hour of the indicated treatments. Rotenone and Antimycin A induce AMPK activation but do not affect Opa1 processing, unlike CCCP.

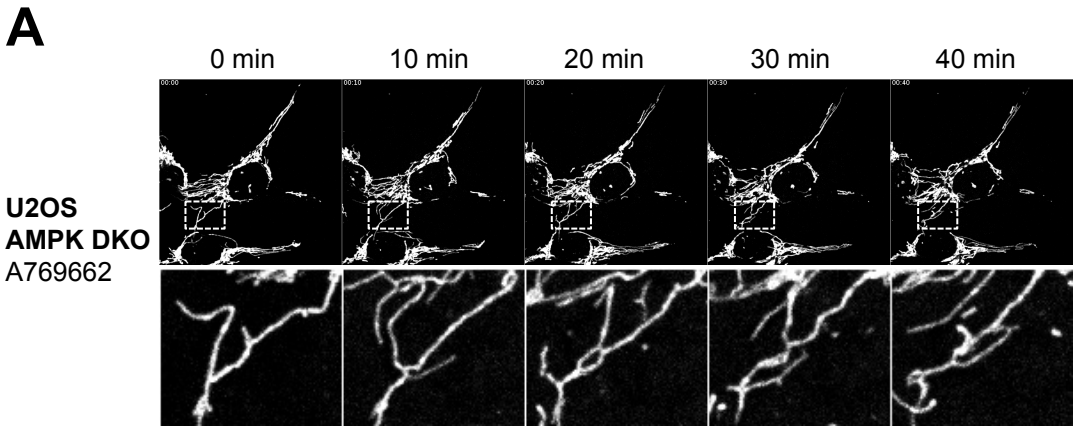

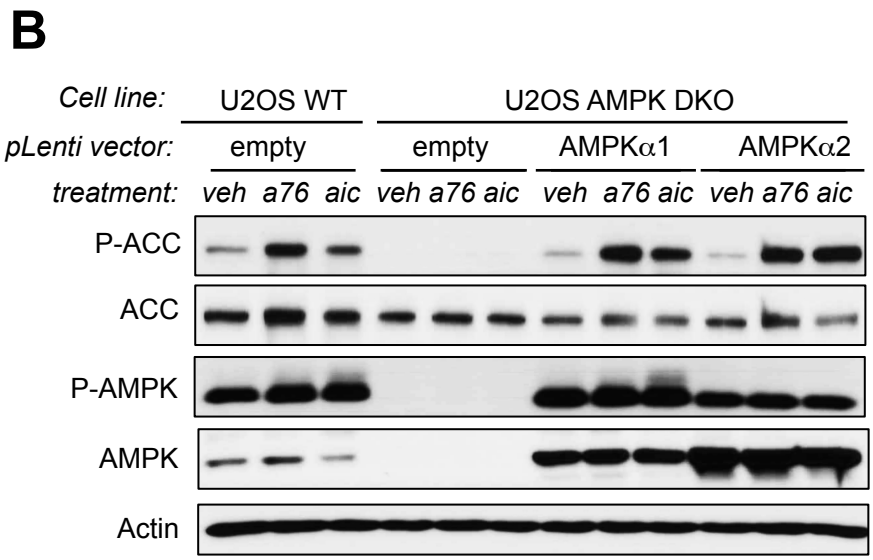

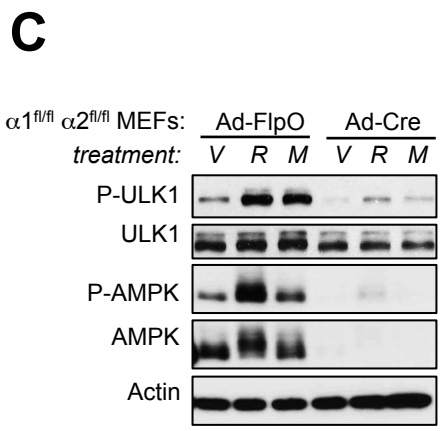

Fig. S2. AMPK is required for mitochondrial fragmentation following A769662 or other AMPK direct activators in the absence of mitochondrial inhibition.

(**A**) Time-lapse images of U2OS AMPK DKO cells stained with MitoTracker Green and treated with 300μM A769662 at 0 minutes. A magnification of a portion of the mitochondrial network (dotted square) is included (bottom panel). (See Movie S5).

(B) Induction of AMPK signaling by A769662 and AICAR is lost in U2OS AMPK DKO cells and rescued by expression of wild-type AMPK α1 or α2 cDNA. Protein immunoblot analysis of cell lines and conditions shown in Fig. 2A and B. veh: Vehicle (DMSO), a76: 300μM A769662, aic: 2mM AICAR.

(**C**) Protein immunoblot of AMPK $\alpha1^{fl/fl}$ $\alpha2^{fl/fl}$ MEFs transduced with FlpO (control) or Cre-encoding Adenoviruses (see Fig. 2D, E) and treated for 1 hour with vehicle (DMSO, V), 100ng/ml Rotenone (R) or 50μM MT68-73 (M).

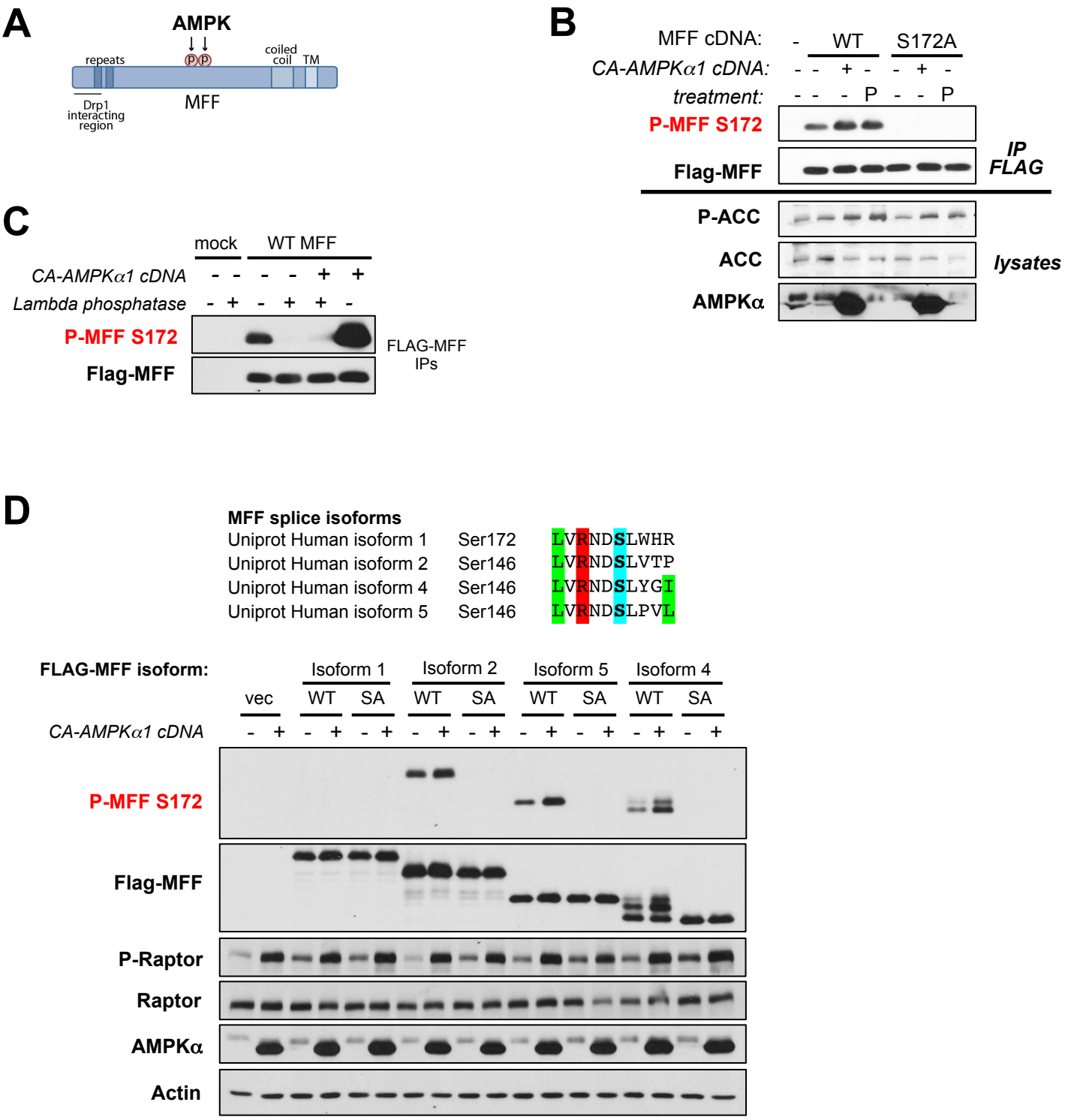

Fig. S3. Validation of pMFF S172 antibody

(**A**) Schematic of MFF cDNA illustrating location of serines 155 and 172 relative to functionally annotated Drp1-binding domains at amino-terminus and transmembrane domain which localizes MFF to outer mitochondrial membrane.

(B) HEK293Ts co-transfected with empty vector (-), WT or MFF S172A mutant and GST (-) or constitutively active GST-AMPKα1 (+ CA-AMPKα1) were treated with vehicle (-) or 2mM phenformin (P) for 1 hour and then lysed. FLAG immunoprecipitations and total cell lysates were immunoblotted as indicated.

(**C**) HEK293Ts co-transfected with empty vector (mock), or WT MFF and GST (-) or constitutively active GST-AMPKα1 (CA-AMPKα1) were lysed and the FLAG immunoprecipitations were treated with lambda phosphatase (+) or left untreated (-) and immunoblotted as indicated.

(**D**) Protein immunoblots of HEK293Ts co-transfected with an empty vector (pcDNA3) or the indicated WT or S172A (SA) human MFF splice isoforms together with GST-constitutively active AMPKα1 (+) or GST alone (-).

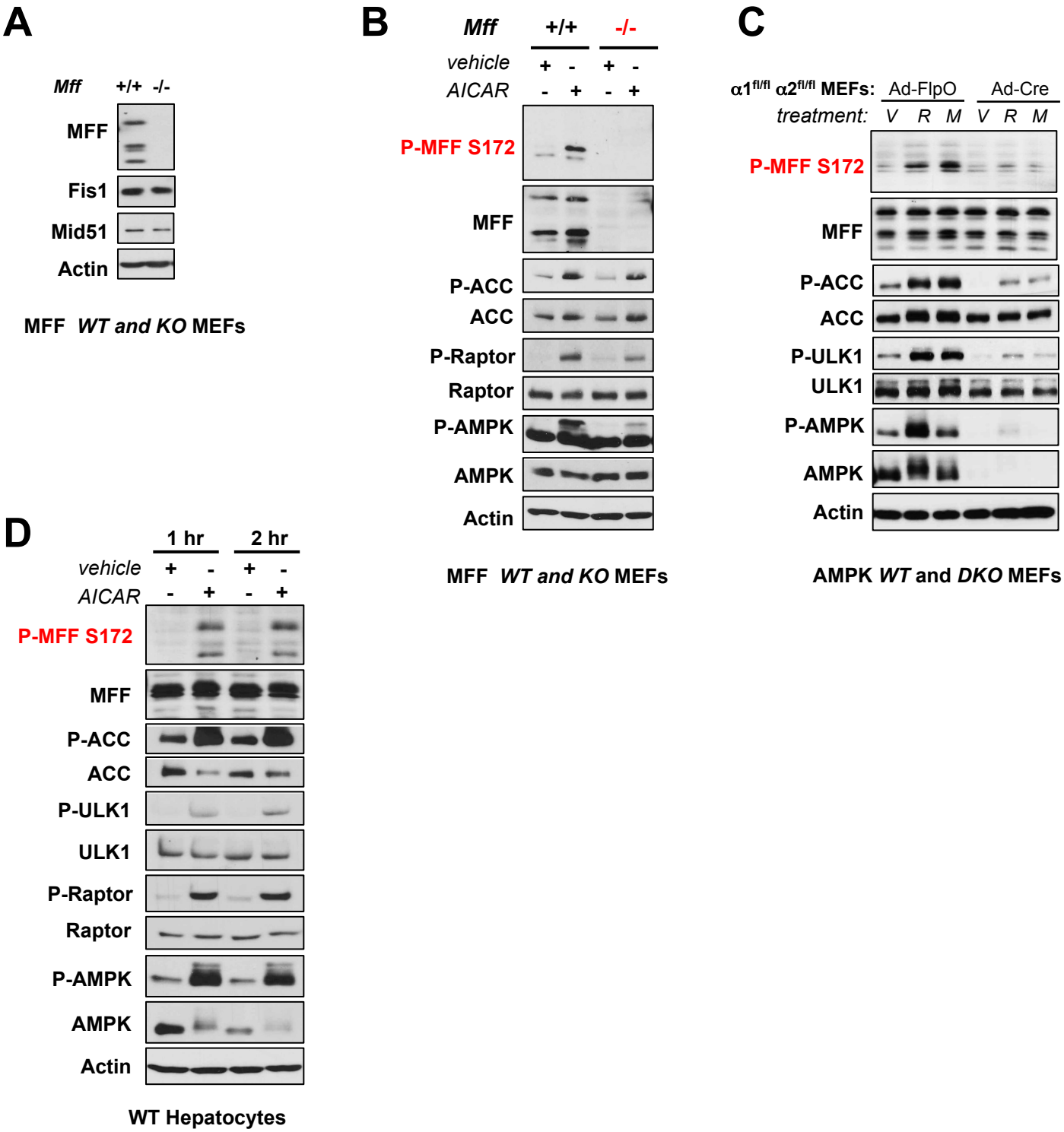

Fig. S4. Analysis of endogenous phosphorylation of MFF^{S172}

(A) Protein immunoblot of *Mff*$^{+/+}$ *and Mff*$^{-/-}$ MEFs for endogenous Drp1 receptors (MFF, Fis1, MiD51)

(B) Protein immunoblot of *Mff*$^{+/+}$ *and Mff*$^{-/-}$ MEFs treated with vehicle or 2mM AICAR for 1hour showing phosphorylation of endogenous MFF as detected by MFF P-Ser^{172}-specific antibody.

(C) Protein immunoblot of WT and AMPK DKO MEFs as in Fig. 2D showing phosphorylation of endogenous MFF 1h after indicated treatments as detected by MFF P-Ser^{172}-specific antibody.
V: Vehicle (DMSO), R: 100ng/ml Rotenone, M: 50mM MT68-73.

(D) Protein immunoblot of WT primary hepatocytes treated with 2mM AICAR for the indicated times showing phosphorylation of endogenous MFF as detected by MFF P-Ser^{172}-specific antibody.

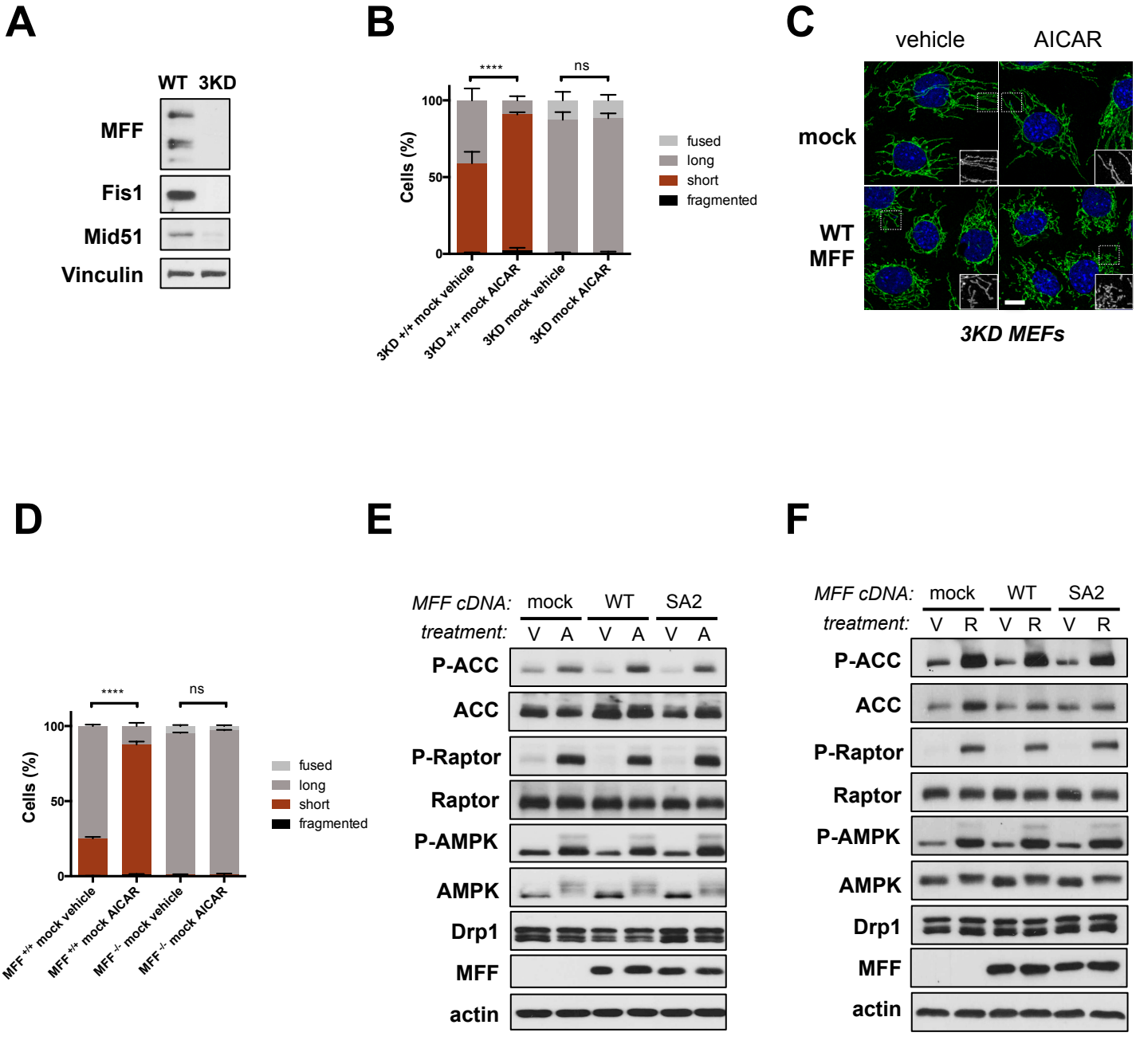

Fig. S5 Analysis of the response of 3KD and *Mff*$^{-/-}$cells with or without re-expression of MFF alleles.
(A) Protein immunoblot of WT or 3KD (*Mff*$^{-/-}$*Fis1*$^{-/-}$ shRNA *Mid51*) MEF cells.
(B) Quantification of mitochondrial morphology WT (+/+) or 3KD (*MFF*$^{-/-}$*Fis1*$^{-/-}$ shRNA Mid51) MEFs transduced with a control vector and treated for 1 hour with vehicle or 2mM AICAR or vehicle (DMSO), fixed and visualized with an antibody to TOM20. Data are shown as mean +/-SEM of three independent experiments with 200 cells counted for each replicate. n.s.: not significant, **: p<0.01, ***: p<0.001 by two-way ANOVA using Tukey's multiple comparisons test for the long and short categories.
(C) Representative images of 3KD cells stably transduced with a control vector (mock) or WT MFF, treated for 1 hour with vehicle or 2mM AICAR, fixed and stained with an antibody to TOM20. Scale bar:10 um.
(D) Quantification of mitochondrial morphology WT or *MFF*$^{-/-}$ MEFs transduced with a control vector and treated for 1 hour with vehicle or 2mM AICAR and quantified as in (B).
(**E**) and (**F**) Protein immunoblots of cell lines from Fig. 4A-C treated for 1h as indicated, demonstrating equivalent AMPK activation and protein levels in all cell lines used. V: Vehicle, A: 2mM AICAR, R: 250ng/ml Rotenone

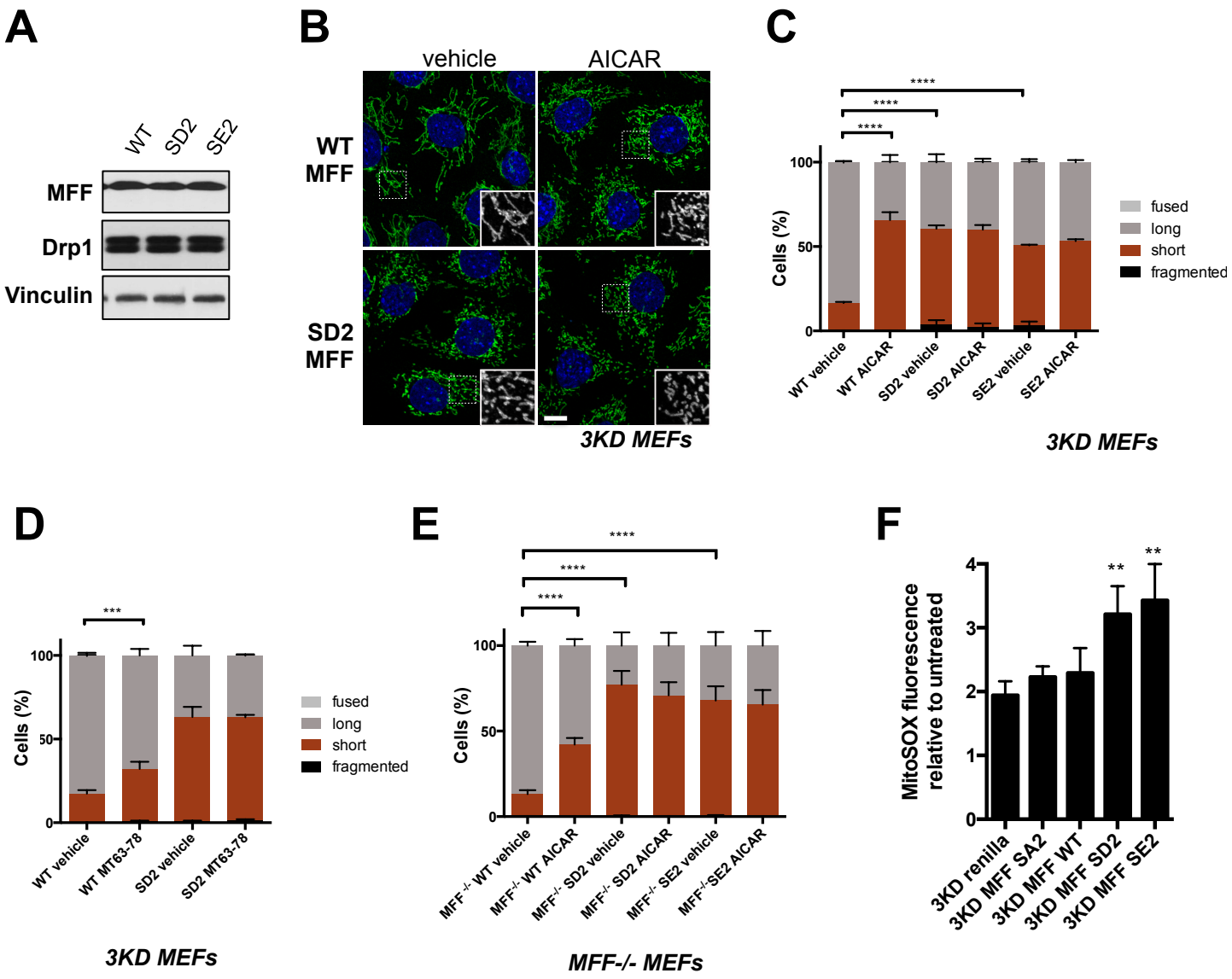

Fig. S6 Phosphomimetic MFF Ser155/Ser 172 alleles behave as gain of function alleles of MFF.
(A) Protein immunoblots of 3KD (MFF-/-Fis1-/- shRNA Mid51 cells) MEFs stably transduced with WT MFF, MFF S155D-S172D (SD2) or MFF S155E-S172E (SE2).
(B) Representative images of 3KD cells stably transduced with WT MFF or MFF S155D-S172D (SD2) treated for 1 hour with vehicle or 2mM AICAR, fixed and stained with an antibody to TOM20. Scale bar:10 um.
(C) Quantification of the mitochondrial morphology of 3KD cells stably transduced with WT MFF or MFF S155D-S172D (SD2) or MFF S155E-S172E (SE2). Data are shown as mean +/-SEM of three independent experiments with 200 cells counted for each replicate. ns: not significant, ***: p<0.001, ****: p<0.0001 by two-way ANOVA using Tukey's multiple comparisons test for the long and short categories.
(D) Quantification of mitochondrial morphology in 3KD MEFs stably transduced with WT or SD2 MFF treated for 1 hour with DMSO (vehicle) or 50µM MT63-78, fixed, visualized with a TOM20 antibody and quantified as in (C).
(E) Quantification of the mitochondrial morphology in MFF $^{-/-}$ MEFs stably transduced with WT MFF or MFF S155D/S172D (SD2) or MFF S155E/S172E (SE2) treated with 2mM AICAR for 1 hour. Data are shown as mean +/-SEM of three independent experiments with at least 200 cells counted for each replicate. ****: p<0.0001 by two-way ANOVA using Tukey's multiple comparisons test for the long and short categories.
(F) Quantification of mitochondrial ROS levels in 3KD MEFs expressing the indicated MFF constructs and treated for 8 hours with 250ng/ml Rotenone. Data are shown as mean +/-SEM of three independent experiments.**: p<0.01, by two-way ANOVA using Tukey's multiple comparisons test.

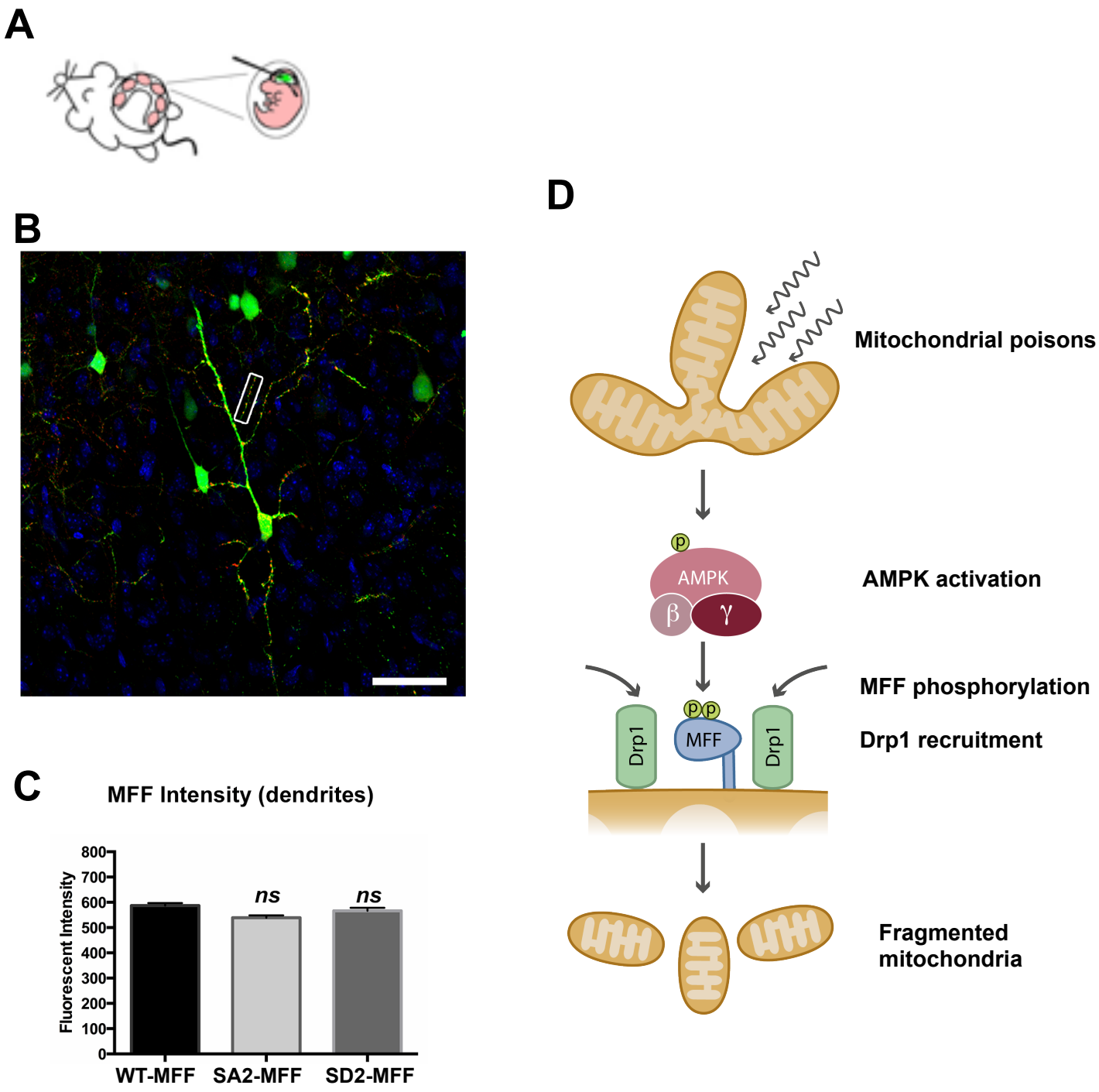

Fig. S7 Analysis of enforced MFF expression in dendrites from cortical neurons in utero electroporated
(A) Schematic illustration of the *in utero* cortical electroporation through microinjection of plasmid constructs in the lateral ventricles of E15.5 mouse embryos.
(B) Max projection image showing a layer 2/3 pyramidal neuron optically isolated by confocal microscopy in the somatosensory cortex at P30 following *in utero* cortical electroporation at E15.5 with the labeled constructs. Hoechst 33258 was used to label all nuclei (Blue), mt-DsRed labels all mitochondria, and mVenus marks cytoplasm of all expressing cells. Small box demonstrates a collateral of the apical dendrite used for quantification of mitochondrial morphology. Scale bar = 50μm
(C) Quantification of FLAG-tagged MFF protein expression in neurons via Flag epitope staining. Data is shown as mean ± s.e.m. $N_{MFF\text{-}WT}$= 556 mitochondria, $N_{MFF\text{-}DD}$=447, $N_{MFF\text{-}AA}$=297 from 10 images per condition. No significant difference (ns) was measured between the three conditions by a non-parametric Kruskal-Wallis Anova test with Dunn's multiple comparisons.
(D) Molecular model for how mitochondrial stress induces AMPK-dependent mitochondrial fragmentation

Material and Methods

Plasmids

MFF (Uniprot Q9GZY8 isoform 5) cDNA was generated by RT-PCR from RNA obtained from IMR90 cells. A single FLAG tag was inserted at the N-terminus of MFF and the resulting product was inserted into pCDNA3, pLenti PGK Blast or pQCXIB Gateway destination vectors. For Figure S3C, Uniprot Q9GZY8 isoform 1, 2, 4 were made as above and inserted into pCDNA3. Mock vectors were generated by amplifying Renilla luciferase by PCR and inserting into pLenti PGK Blast or pQCXIB Gateway destination vectors. MFF phosphorylation site mutants were generated by PCR. pEBG-AMPKα1(amino acids 1α312) is constitutively active by truncation after amino acid 312 as described previously (*27*). Untagged human AMPKα1 or AMPKα2 cDNAs were inserted into pCMV/TO puro Gateway destination vector.

Reagents and antibodies

The following antibodies were used: actin (A5441), ULK1 (A7481) and Flag (F7425) from Sigma, TOM20 (FL-145, Santa Cruz), Drp1 (611113, BD Biosciences), and MFF (17090-1-AP, Protein Tech). The following antibodies were from Cell Signaling Technologies: pAMPK Thr172 (#2535), AMPK α1/2 (#2532), pACC Ser79 (#3661), ACC (#3662), pRaptor Ser792 (#2083), Raptor (#2280), pULK1 Ser555 (#5869), phospho(Ser)14-3-3 binding motif (#9601), pAMPK substrate motif (#5759S). phospho-MFF S172 was developed in collaboration with Amrik Singh and Gary Kasof at Cell Signaling Technologies. The following secondary antibodies were used: Alexa488 goat anti-rabbit (A11070), Alexa 488 goat anti-mouse (A11017), Alexa 568 goat anti-rabbit (A11034) from Life Technologies and HRP-coupled antibodies to mouse (AP124P) and rabbit (AP132P) from Millipore.AICARwas obtained from Toronto Research Chemicals, A769662 from Reagents Direct and Phenformin, Metformin, Rotenone, Antimycin A from Sigma. MT68-73 was from a kind gift from Dr. Massimo Loda (Harvard Medical School) (*25*).

Cell lines

WT and MFF $^{-/-}$ MEFS were generated as in (*31*). To generate the 3 KD MEFs, *Fis1*/*Mff*-null MEFs (*31*) were transduced with retrovirus carrying *MiD51* shRNA. Transduced cells were selected for viral integration using puromycin resistance. The *MiD51* shRNA vector was generated by annealing and subcloning oligonucleotides (5' GATCTGCTGTCATTCTTTGTCATAAACTCGAGTTTATGACAAAGAATGACAGCTTTTT G 3' and 5' AATTCAAAAAGCTGTCATTCTTTGTCATAAACTCGAGTTTATGACAAAGAATGACAG CA 3') into the EcoRI and BglII sites of pRetroX (Life Technologies).

AMPKα1 (*Prkaa1*) $^{fl/fl}$ and AMPKα2 (*Prkaa2*) $^{fl/fl}$ mice were obtained from Benoit Viollet (Institut Cochin, INSERM, Université Paris Descartes) and interbred to create double floxed *Prkaa1*$^{fl/fl}$ *Prkaa2*$^{fl/fl}$ mice from which MEFs were derived as previously described (*15*). AMPK

$\alpha1^{fl/fl}$ $\alpha2^{fl/fl}$ MEFs were immortalized with SV40 T antigen and were transduced with adenovirus encoding FlpO (control) or Cre recombinase and used at least 1 week post-transduction. Wild-type and AMPK $\alpha1^{-/-}$, $\alpha2^{-/-}$ double knockout MEFs were previously described (*27*). SV40 immortalized wild-type MEFs used in Figure 3D were described previously (*15*). All cell lines were cultured in DMEM (Corning #10-013-CV) containing 4.5 g/L glucose, pyruvate and L-glutamine supplemented with 10% FBS (Hyclone) and Penicillin/Streptomycin (Gibco) in a 37°C incubator with 10% (U2OS, AMPK $\alpha1^{fl/fl}$ $\alpha2^{fl/fl}$ MEFs) or 5% (3KD MEFs) CO_2.
For primary hepatocytes, AMPK $\alpha1^{fl/fl}$/$\alpha2^{fl/fl}$ FVB mice with or without Albumin-CreER expression were injected 3x every other day with 1mg/kg tamoxifen. 17days later primary hepatocytes were isolated by perfusing livers with Hank's balanced salt solution (HBSS, KCl, 5.4 mM;KH2 PO4 ,0.44mM; NaCl, 138mM; NaHCO3 ,4.2 mM; Na2HPO4, 0.34 mM; glucose, 5.6 mM; HEPES, 55 mM; EGTA, 0.6 mM; pH 7.4). Livers were washed at a rate of 5 ml/min using the vena cava before switching to collagenase buffer (same as above but without EGTA and supplemented with CaCl2, 5 mM; Collagenase (Sigma C5138); 0.025%)). Cell viability was assessed by the trypan blue exclusion test and was higher than 75%. $1.8*10^6$ hepatocytes were seeded in DMEM medium (Corning, 10-017), supplemented with 5%FBS, and penicillin/ streptomycin onto 60mm TPP plates (Light Lab Systems). After cell attachment (4 h), the medium was replaced by fresh DMEM medium with 5% FBS and the experiments were performed the following day.

Transfection and Virus Production

Lentiviral and retroviral infection was performed as described previously (*36*). Wild-type MEFs were stably transduced with pQXCIB expressing Flag-MFF, FLAG-MFF mutants, or Renilla luciferase by retroviral infection and selected using blasticidin (Life Technologies). Matched wild-type and AMPK $\alpha1^{-/-}$, $\alpha2^{-/-}$ MEFs and wild-type and 3KD MEFs were stably transduced with pLenti PGK expressing FLAG-MFF, MFF mutants, or Renilla by lentiviral infection and selected using blasticidin. Stable re-expression of AMPK $\alpha1$ or $\alpha2$ into U2OS AMPK $\alpha1$ $\alpha2$ DKO cells was performed using lentivirus-mediated transduction of the human untagged gene cloned into pCMV/TO vector and selected with puromycin (Sigma). Transient transfections were done using Lipofectamine 2000 (Life Technologies) according to manufacturer's instructions. Transfected cell lysates were harvested 20-24 hours post transfection.

Cell lysis and immunoprecipitation

At indicated timepoints after changing the media with fresh media containing vehicle or drug treatment, cells were washed with cold PBS and lysed in lysis buffer: 20 mM Tris pH 7.5, 150 mM NaCl, 1 mM EDTA, 1mM EGTA, 1% Triton X-100, 2.5 mM pyrophosphate, 50 mM NaF, 5 mM β-glycero-phosphate, 50 nM calyculin A, 1 mM Na3VO4, and protease inhibitors (Roche). For timecourse experiments, media was changed for 1 hour prior to the addition of the drug treatment and cells were lysed at the indicated times. Lysates were incubated at 4°C for 15 minutes and cleared at 16,000g for 15 minutes at 4°C. Total protein was normalized using BCA

protein kit (Pierce) and lysates were resolved on SDS-PAGE gel. Immunoprecipitations were performed by adding M2 FLAG agarose (Sigma) to equilibrated lysates for 1.5 hours at 4°C. The beads were washed three times with lysis buffer and then eluted by boiling in SDS lysis buffer for 5 minutes and resolved by SDS-PAGE gel.
For lambda phosphatase assays, HEK293Ts transiently co-transfected with FLAG-MFFand pEBG-CA-AMPKα1 and were lysed and subjected to FLAG-immunoprecipitation. Immunoprecipitates were washed three times in lysis buffer and then three times in Protein MetalloPhosphatase buffer (NEB) and then added to the phosphatase reaction with or without 2ul lambda phosphatase (NEB). The reaction was incubated at 30°C for 30 minutes and then washed, treated with SDS sample buffer, boiled and resolved by SDS-PAGE gel.

Kinase assays

Radioactive in vitro kinase assays were performed essentially as described in (*15*) with minor modifications. Briefly, HEK293Ts transiently transfected with FLAG-MFF were lysed and subjected to FLAG-immunoprecipitation. Immunoprecipitates were washed three times in lysis buffer and then three times in kinase buffer (50 mM Tris pH 7.5 10 mM $MgCl_2$) and added to the kinase reaction containing ATP $\gamma^{32}P$ and 2mM DTT with or without 50ng of active recombinant AMPK (Millipore #14-840). The reaction was incubated for 5 minutes at 37°C and processed as described in (*15*).

Immunofluorescence

For analysis of mitochondrial morphology, U2OS cells were grown overnight on glass coverslips, the media was replaced with fresh media containing drug or vehicle, incubated for 1 hour, fixed in 4% PFA (Electron microscopy sciences) for 15 minutes at room temperature, permeabilized with 0.1% Triton X-100, blocked in 5% BSA and stained with antibodies to TOM20 followed by Alexa488-labelled secondary antibodies and counterstained with DAPI. Coverslips were mounted using ProlongGold (Life Technologies). 3KD and *Mff*$^{-/-}$ MEFs were treated similarly except that the cells were fixed at 37°C for 15 minutes, blocked using 5% FBS and the coverslips were mounted using Fluoromount G (Southern Biotech). Cells were imaged using a Zeiss LSM 700 confocal microscope. For quantification of mitochondrial morphology of TOM20-stained cells, scoring was done blind to genotype and treatment. "Fragmented" was defined as cells in which the majority of mitochondria were spherical (no clear length or width); "Short" were cells with a majority of mitochondria less than ~10 um; "Long" were cells in which the majority of mitochondria were more than ~10 um, and "Fused" was defined as cells with highly interconnected mitochondria with less than 4-5 free ends.

Mitochondrial Drp1 colocalization analysis

Cells were processed for immunofluorescence as described above and stained with antibodies to TOM20 (FL-145, Santa Cruz) and Drp1 (611113, BD Biosciences) followed by detection using

Alexa 488 anti-mouse and Alexa 568 anti-rabbit secondaries. Images were acquired on a Zeiss 700 confocal microscope at 63x using constant acquisition settings across samples blinded for genotype and treatment. Images were then analyzed in ImageJ using the colocalization highlighter plugin. To generate the colocalization score, images were converted to 8 bits, thresholded and the number of white pixels, indicating colocalization, were counted using analyze particle and normalized to the total mitochondrial area in each picture. A total of 4 independent experiments consisting of at least 5 pictures, representing at least 40 cells per condition, were used for each sample.

Time-lapse microscopy

U2OS cells were plated in glass chamber slides (LabTek) and stained for 30min with 100nM MitoTracker Green (Life Technologies) before addition of the drug. Imaging was started immediately after addition of the drug on a Zeiss CSU spinning disc confocal at 37°C and 10% CO_2. 6 z-stacks were acquired every 5 min for 2 hours. After acquisition, maximal projection of the z-stack was performed using ImageJ and exported as uncompressed AVI sequences at 2 frames per second.

Seahorse assay

Dose response of Rotenone in WT and AMPK DKO U2OS cells measured with a Seahorse flux analyzer. Oxygen consumption 3 min after drug addition was normalized to the value immediately before the addition of the drug and is shown as a function of drug concentration (log scale).

Primary neuronal culture and *ex utero* electroporation

Cortices from E15.5 CD1 mouse embryos were dissected in Hanks' Buffered Salk Solution (HBSS) supplemented with Hepes (2.5 mM), $CaCl_2$ (1 mM, Sigma), $MgSO_4$ (1 mM, Sigma), $NaHCO_3$ (4mM, Sigma) and D-glucose (30 mM, Sigma), hereafter referred to as cHBSS. Cortices were dissociated in cHBSS containing papain (Worthington) and DNAse I (100 µg/ml, Sigma) for 20 min at 37°C, washed three times and manually triturated in cHBSS supplemented with DNAse. Cells were then plated at 7.5 x 10^4 cells per 35mm glass bottom dish (Matek) coated with poly-D-lysine (1 mg/ml, Sigma) and cultured for 21 days in neurobasal medium supplemented with B27 (1X), FBS (2.5%), L-glutamine (2 mM). One third of the medium was changed every 5 days thereafter with non-FBS containing medium. *Ex utero* electroporation (pSCV2 mVenus -0.75µg/µL, pCAG mito-DSRED - .25µg/µL, 1µg/µL pCAG Renilla, of MFF-WT/AA/DD (final concentration 2µg/µL)) was performed as previously published in Courchet et al (2013). Cells were fixed and stained as previously published (*36*). Antibodies used were chicken anti-GFP (Aves, 1:2000), rabbit anti-RFP (Abcam, 1:1000), mouse anti-Flag (Sigma, 1:500).

In utero electroporation

In utero electroporations were performed as detailed in (*36*) with the exception that CD1 mice were used. Briefly, a mix of endotoxin-free plasmid preparation (pSCV2 mVenus -0.75μg/μL, pCAG mito-DSRED - .25μg/μL, 1μg/μL pCAG Renilla, of MFF-WT/AA/DD (final concentration 2μg/μL)) was injected into one lateral hemisphere of E15.5 embryos using a picospritzer. Electroporation was performed with gold paddles to target cortical progenitors in E15.5 embryos by placing the anode (positively charged electrode) on the side of DNA injection and the cathode on the other side of the head. Four pulses of 45 V for 50 ms with 500 ms interval were used for electroporation. Animals were sacrificed 30 days after birth by terminal perfusion of 4% paraformaldehyde (PFA, Electron Microscopy Sciences) followed by 2 hours post-fixation in 4% PFA. Staining was performed as previously published (*36*). Antibodies used were chicken anti-GFP (Aves, 1:2000), rabbit anti-RFP (Abcam, 1:1000), mouse anti-Flag (Sigma, 1:500). Hoechst 33528 (Invitrogen, 1:10000) was used to label nuclei.

Mouse Neuron Imaging and Quantification

Confocal imaging was performed on a Nikon Ti-e inverted microscope using Nikon's A1 confocal, Nikon NIS-Elements and a 100x 1.49NA Nikon objective. Nikon's NIS-Elements Advanced Research program was used to draw regions of interest (ROI) around individual mitochondria along collaterals of the apical dendrite. Elements then extracted area and intensity from each ROI. All analysis was performed blind to the observer by randomization with a random number generator. All statistical analysis was performed in Prism.

Mitochondrial ROS measurement

Mitochondrial ROS levels were measured using the MitoSOX probe (Life Technologies). Following treatment with Rotenone for 7h and loading with 2.5μM MitoSOX for 30 minutes, cells were trypsinized, resuspended in HBSS and immediately analyzed by FACS in a Canto II analyzer.

Knockout cell generation using CRISPR

Knockouts were generated using the Cas9 nickase strategy as described (*40*). Briefly, a pair of guide RNAs (gRNA) targeting the exon 1 was designed for both human PRKAA1 and PRKAA2 genes using the online design tool at crispr.mit.edu (AMPK α1 A/B and AMPK α2 A/B, respectively). Each gRNA duplex was cloned into pX462 vector encoding SpCas9n-2A-puro (Addgene # 48141). U2OS cells were transfected with the gRNA pair to generate single α1 or α2 KO or transfected with both pairs together to generate double α1/ α2 KO (DKO). After puromycin selection, single cell cloning was performed by cell sorting into 96-well plates. Individual clones were screened by western blot and a clone lacking both AMPK α1 and α2 protein expression was selected.

gRNA sequences

AMPK α1 A: GGCTGTCGCCATCTTTCTCC, B: GAAGATCGGCCACTACATTC

AMPK α2 A: TCAGCCATCTTCGGCGCGCG, B: GAAGATCGGACACTACGTGC

Sequencing of CRISPR alleles

A region at the 5' end of both PRKAA1 and PRKAA2 genes was PCR amplified using primers hA1F: GCTCTCGTAACAAGCCACAG, hA1R: CCAGCCCTGGAAAGAAGG, hA2F: TCCTCAGAAAGGGCCTCCT, hA2R: GACCTCCAGAAAGGCAGATG. The PCR products were TOPO cloned using Zero Blunt TOPO PCR cloning kit (Life Technologies) according to the manufacturers instructions. A total of 40 clones were mini prepped and sequenced by Sanger sequencing and aligned to the reference sequence. This revealed that the PRKAA1 gene was modified as follow: an insertion of 41 bp and 19 at positions +28 and +33 relative to the start codon, respectively; a deletion of 26 bp starting at +26; and an insertion of 78 bp at position +73. The PRKAA2 alleles were a deletion of 96 bp starting at position -37 relative to the start codon; and an insertion of 25bp at position +11 and a deletion of 33bp at position +26. All these alleles disrupt the open reading frame and result in premature stop codons.

Supplemental text re: MFF alternative splicing

The MFF gene encodes a number of alternative splice isoforms, several of which were described when it was first identified (*30*). However, only a few of these splice isoforms are well annotated in Uniprot. Notably, one splice junction lies just carboxyl-terminal to one of the two AMPK phosphorylation sites (Ser^{172} in human MFF isoform 1), and this alternative splicing changes the amino acid residues that follow the serine phosphorylated by AMPK (see lineup below). One potential impact of these sequence changes is that the different MFF splice isoforms may differ in their ability to be phosphorylated by AMPK, with isoforms bearing weaker AMPK substrate sequence motifs being potentially less robustly phosphorylated by AMPK *in vivo*. It should be pointed out, though, that the second AMPK phosphorylation site, Ser^{155}, is present in all MFF splice isoforms, and AMPK should therefore be capable of phosphorylating all MFF splice isoforms at this site. We cannot predict a priori whether the MFF isoforms that fit the AMPK substrate motif less optimally are actually less stoichimetrically phosphorylated *in vivo* since much of the AMPK sequence selectivity is still present at Ser^{172}, while a second, perfect AMPK site (Ser^{155}) still exists in MFF, which may serve to recruit AMPK to phosphorylate MFF at both sites regardless of how well Ser^{172} conforms to the predicted, optimal AMPK motif. One additional impact of the differential splicing surrounding Ser^{172} is that different MFF splice isoforms may be more or less reactive to the phospho-antibody we generated against P-Ser^{172}, which was generated against a peptide corresponding to Ser^{172} in MFF isoform 2. This may explain why our P-Ser^{172} antibody does not recognize the higher molecular weight MFF isoforms 1 and 3 in MEFs, which express several different splice isoforms of distinct molecular weights (see Fig. 3F, S3B, S3C). Lastly, it is worth noting that these alternative splice isoforms appear fully conserved to mouse and may extend further back through evolution given that MFF itself is conserved back to C. elegans (*30*).

REFERENCES AND NOTES

1. P. Mishra, D. C. Chan, Mitochondrial dynamics and inheritance during cell division, development and disease. *Nat. Rev. Mol. Cell Biol.* **15**, 634–646 (2014). Medline doi:10.1038/nrm3877

2. G. Benard, N. Bellance, D. James, P. Parrone, H. Fernandez, T. Letellier, R. Rossignol, Mitochondrial bioenergetics and structural network organization. *J. Cell Sci.* **120**, 838–848 (2007). Medline doi:10.1242/jcs.03381

3. G. Twig, A. Elorza, A. J. Molina, H. Mohamed, J. D. Wikstrom, G. Walzer, L. Stiles, S. E. Haigh, S. Katz, G. Las, J. Alroy, M. Wu, B. F. Py, J. Yuan, J. T. Deeney, B. E. Corkey, O. S. Shirihai, Fission and selective fusion govern mitochondrial segregation and elimination by autophagy. *EMBO J.* **27**, 433–446 (2008). Medline doi:10.1038/sj.emboj.7601963

4. S. Montessuit, S. P. Somasekharan, O. Terrones, S. Lucken-Ardjomande, S. Herzig, R. Schwarzenbacher, D. J. Manstein, E. Bossy-Wetzel, G. Basañez, P. Meda, J. C. Martinou, Membrane remodeling induced by the dynamin-related protein Drp1 stimulates Bax oligomerization. *Cell* **142**, 889–901 (2010). Medline doi:10.1016/j.cell.2010.08.017

5. M. Karbowski, Y. J. Lee, B. Gaume, S. Y. Jeong, S. Frank, A. Nechushtan, A. Santel, M. Fuller, C. L. Smith, R. J. Youle, Spatial and temporal association of Bax with mitochondrial fission sites, Drp1, and Mfn2 during apoptosis. *J. Cell Biol.* **159**, 931–938 (2002). Medline doi:10.1083/jcb.200209124

6. R. J. Youle, M. Karbowski, Mitochondrial fission in apoptosis. *Nat. Rev. Mol. Cell Biol.* **6**, 657–663 (2005). Medline doi:10.1038/nrm1697

7. D. R. Green, L. Galluzzi, G. Kroemer, Metabolic control of cell death. *Science* **345**, 1250256 (2014). Medline doi:10.1126/science.1250256

8. J. Q. Kwong, M. S. Henning, A. A. Starkov, G. Manfredi, The mitochondrial respiratory chain is a modulator of apoptosis. *J. Cell Biol.* **179**, 1163–1177 (2007). Medline doi:10.1083/jcb.200704059

9. M. Liesa, O. S. Shirihai, Mitochondrial dynamics in the regulation of nutrient utilization and energy expenditure. *Cell Metab.* **17**, 491–506 (2013). Medline doi:10.1016/j.cmet.2013.03.002

10. L. C. Gomes, G. Di Benedetto, L. Scorrano, During autophagy mitochondria elongate, are spared from degradation and sustain cell viability. *Nat. Cell Biol.* **13**, 589–598 (2011). Medline doi:10.1038/ncb2220

11. A. S. Rambold, B. Kostelecky, N. Elia, J. Lippincott-Schwartz, Tubular network formation protects mitochondria from autophagosomal degradation during nutrient starvation. *Proc. Natl. Acad. Sci. U.S.A.* **108**, 10190–10195 (2011). Medline doi:10.1073/pnas.1107402108

12. A. S. Rambold, S. Cohen, J. Lippincott-Schwartz, Fatty acid trafficking in starved cells: Regulation by lipid droplet lipolysis, autophagy, and mitochondrial fusion dynamics. *Dev. Cell* **32**, 678–692 (2015). Medline doi:10.1016/j.devcel.2015.01.029

13. B. B. Kahn, T. Alquier, D. Carling, D. G. Hardie, AMP-activated protein kinase: Ancient energy gauge provides clues to modern understanding of metabolism. *Cell Metab.* **1**, 15–25 (2005). Medline doi:10.1016/j.cmet.2004.12.003

14. M. M. Mihaylova, R. J. Shaw, The AMPK signalling pathway coordinates cell growth, autophagy and metabolism. *Nat. Cell Biol.* **13**, 1016–1023 (2011). Medline doi:10.1038/ncb2329

15. D. F. Egan, D. B. Shackelford, M. M. Mihaylova, S. Gelino, R. A. Kohnz, W. Mair, D. S. Vasquez, A. Joshi, D. M. Gwinn, R. Taylor, J. M. Asara, J. Fitzpatrick, A. Dillin, B. Viollet, M. Kundu, M. Hansen, R. J. Shaw, Phosphorylation of ULK1 (hATG1) by AMP-activated protein kinase connects energy sensing to mitophagy. *Science* **331**, 456–461 (2011). Medline doi:10.1126/science.1196371

16. J. Kim, M. Kundu, B. Viollet, K. L. Guan, AMPK and mTOR regulate autophagy through direct phosphorylation of Ulk1. *Nat. Cell Biol.* **13**, 132–141 (2011). Medline doi:10.1038/ncb2152

17. P. Mishra, V. Carelli, G. Manfredi, D. C. Chan, Proteolytic cleavage of Opa1 stimulates mitochondrial inner membrane fusion and couples fusion to oxidative phosphorylation. *Cell Metab.* **19**, 630–641 (2014). Medline doi:10.1016/j.cmet.2014.03.011

18. S. Ehses, I. Raschke, G. Mancuso, A. Bernacchia, S. Geimer, D. Tondera, J. C. Martinou, B. Westermann, E. I. Rugarli, T. Langer, Regulation of OPA1 processing and mitochondrial fusion by m-AAA protease isoenzymes and OMA1. *J. Cell Biol.* **187**, 1023–1036 (2009). Medline doi:10.1083/jcb.200906084

19. N. Ishihara, Y. Fujita, T. Oka, K. Mihara, Regulation of mitochondrial morphology through proteolytic cleavage of OPA1. *EMBO J.* **25**, 2966–2977 (2006). Medline doi:10.1038/sj.emboj.7601184

20. B. Head, L. Griparic, M. Amiri, S. Gandre-Babbe, A. M. van der Bliek, Inducible proteolytic inactivation of OPA1 mediated by the OMA1 protease in mammalian cells. *J. Cell Biol.* **187**, 959–966 (2009). Medline

21. S. Duvezin-Caubet, R. Jagasia, J. Wagener, S. Hofmann, A. Trifunovic, A. Hansson, A. Chomyn, M. F. Bauer, G. Attardi, N. G. Larsson, W. Neupert, A. S. Reichert, Proteolytic processing of OPA1 links mitochondrial dysfunction to alterations in mitochondrial morphology. *J. Biol. Chem.* **281**, 37972–37979 (2006). Medline

22. K. R. Laderoute, K. Amin, J. M. Calaoagan, M. Knapp, T. Le, J. Orduna, M. Foretz, B. Viollet, 5′-AMP-activated protein kinase (AMPK) is induced by low-oxygen and glucose deprivation conditions found in solid-tumor microenvironments. *Mol. Cell. Biol.* **26**, 5336–5347 (2006). Medline doi:10.1128/MCB.00166-06

23. B. Cool, B. Zinker, W. Chiou, L. Kifle, N. Cao, M. Perham, R. Dickinson, A. Adler, G. Gagne, R. Iyengar, G. Zhao, K. Marsh, P. Kym, P. Jung, H. S. Camp, E. Frevert, Identification and characterization of a small molecule AMPK activator that treats key components of type 2 diabetes and the metabolic syndrome. *Cell Metab.* **3**, 403–416 (2006). Medline doi:10.1016/j.cmet.2006.05.005

24. B. Xiao, M. J. Sanders, D. Carmena, N. J. Bright, L. F. Haire, E. Underwood, B. R. Patel, R. B. Heath, P. A. Walker, S. Hallen, F. Giordanetto, S. R. Martin, D. Carling, S. J.

Gamblin, Structural basis of AMPK regulation by small molecule activators. *Nat. Commun.* **4**, 3017 (2013). Medline doi:10.1038/ncomms4017

25. G. Zadra, C. Photopoulos, S. Tyekucheva, P. Heidari, Q. P. Weng, G. Fedele, H. Liu, N. Scaglia, C. Priolo, E. Sicinska, U. Mahmood, S. Signoretti, N. Birnberg, M. Loda, A novel direct activator of AMPK inhibits prostate cancer growth by blocking lipogenesis. *EMBO Mol. Med.* **6**, 519–538 (2014). Medline doi:10.1002/emmm.201302734

26. M. F. Calabrese, F. Rajamohan, M. S. Harris, N. L. Caspers, R. Magyar, J. M. Withka, H. Wang, K. A. Borzilleri, P. V. Sahasrabudhe, L. R. Hoth, K. F. Geoghegan, S. Han, J. Brown, T. A. Subashi, A. R. Reyes, R. K. Frisbie, J. Ward, R. A. Miller, J. A. Landro, A. T. Londregan, P. A. Carpino, S. Cabral, A. C. Smith, E. L. Conn, K. O. Cameron, X. Qiu, R. G. Kurumbail, Structural basis for AMPK activation: Natural and synthetic ligands regulate kinase activity from opposite poles by different molecular mechanisms. *Structure* **22**, 1161–1172 (2014). Medline

27. D. M. Gwinn, D. B. Shackelford, D. F. Egan, M. M. Mihaylova, A. Mery, D. S. Vasquez, B. E. Turk, R. J. Shaw, AMPK phosphorylation of raptor mediates a metabolic checkpoint. *Mol. Cell* **30**, 214–226 (2008). Medline doi:10.1016/j.molcel.2008.03.003

28. M. M. Mihaylova, D. S. Vasquez, K. Ravnskjaer, P. D. Denechaud, R. T. Yu, J. G. Alvarez, M. Downes, R. M. Evans, M. Montminy, R. J. Shaw, Class IIa histone deacetylases are hormone-activated regulators of FOXO and mammalian glucose homeostasis. *Cell* **145**, 607–621 (2011). Medline doi:10.1016/j.cell.2011.03.043

29. Y. Li, S. Xu, M. M. Mihaylova, B. Zheng, X. Hou, B. Jiang, O. Park, Z. Luo, E. Lefai, J. Y. Shyy, B. Gao, M. Wierzbicki, T. J. Verbeuren, R. J. Shaw, R. A. Cohen, M. Zang, AMPK phosphorylates and inhibits SREBP activity to attenuate hepatic steatosis and atherosclerosis in diet-induced insulin-resistant mice. *Cell Metab.* **13**, 376–388 (2011). Medline

30. S. Gandre-Babbe, A. M. van der Bliek, The novel tail-anchored membrane protein Mff controls mitochondrial and peroxisomal fission in mammalian cells. *Mol. Biol. Cell* **19**, 2402–2412 (2008). Medline doi:10.1091/mbc.E07-12-1287

31. O. C. Losón, Z. Song, H. Chen, D. C. Chan, Fis1, Mff, MiD49, and MiD51 mediate Drp1 recruitment in mitochondrial fission. *Mol. Biol. Cell* **24**, 659–667 (2013). Medline doi:10.1091/mbc.E12-10-0721

32. Q. Shen, K. Yamano, B. P. Head, S. Kawajiri, J. T. Cheung, C. Wang, J. H. Cho, N. Hattori, R. J. Youle, A. M. van der Bliek, Mutations in Fis1 disrupt orderly disposal of defective mitochondria. *Mol. Biol. Cell* **25**, 145–159 (2014). Medline doi:10.1091/mbc.E13-09-0525

33. H. Otera, C. Wang, M. M. Cleland, K. Setoguchi, S. Yokota, R. J. Youle, K. Mihara, Mff is an essential factor for mitochondrial recruitment of Drp1 during mitochondrial fission in mammalian cells. *J. Cell Biol.* **191**, 1141–1158 (2010). Medline doi:10.1083/jcb.201007152

34. S. Ducommun, M. Deak, D. Sumpton, R. J. Ford, A. Núñez Galindo, M. Kussmann, B. Viollet, G. R. Steinberg, M. Foretz, L. Dayon, N. A. Morrice, K. Sakamoto, Motif affinity and mass spectrometry proteomic approach for the discovery of cellular AMPK

targets: Identification of mitochondrial fission factor as a new AMPK substrate. *Cell. Signal.* **27**, 978–988 (2015). Medline doi:10.1016/j.cellsig.2015.02.008

35. X. Qi, N. Qvit, Y. C. Su, D. Mochly-Rosen, A novel Drp1 inhibitor diminishes aberrant mitochondrial fission and neurotoxicity. *J. Cell Sci.* **126**, 789–802 (2013). Medline doi:10.1242/jcs.114439

36. J. Courchet, T. L. Lewis Jr., S. Lee, V. Courchet, D. Y. Liou, S. Aizawa, F. Polleux, Terminal axon branching is regulated by the LKB1-NUAK1 kinase pathway via presynaptic mitochondrial capture. *Cell* **153**, 1510–1525 (2013). Medline doi:10.1016/j.cell.2013.05.021

37. G. Mairet-Coello, J. Courchet, S. Pieraut, V. Courchet, A. Maximov, F. Polleux, The CAMKK2-AMPK kinase pathway mediates the synaptotoxic effects of Aβ oligomers through Tau phosphorylation. *Neuron* **78**, 94–108 (2013). Medline doi:10.1016/j.neuron.2013.02.003

38. R. J. Youle, A. M. van der Bliek, Mitochondrial fission, fusion, and stress. *Science* **337**, 1062–1065 (2012). Medline doi:10.1126/science.1219855

39. J. W. Scott, D. G. Norman, S. A. Hawley, L. Kontogiannis, D. G. Hardie, Protein kinase substrate recognition studied using the recombinant catalytic domain of AMP-activated protein kinase and a model substrate. *J. Mol. Biol.* **317**, 309–323 (2002). Medline doi:10.1006/jmbi.2001.5316

40. F. A. Ran, P. D. Hsu, J. Wright, V. Agarwala, D. A. Scott, F. Zhang, Genome engineering using the CRISPR-Cas9 system. *Nat. Protoc.* **8**, 2281–2308 (2013). Medline doi:10.1038/nprot.2013.143